Internal Dynamics of the Generation of Atmospheric Teleconnection Patterns

Li Zhijin (李志锦) and *Ji Liren* (纪立人)
Institute of Atmospheric Physics, Chinese Academy of Sciences, Beijing 100080
Received December 27, 1994; revised August 21, 1995

ABSTRACT

A preferred growing perturbation concept has been introduced into the dynamical study on the generation of atmospheric teleconnection patterns. It is shown that all the important teleconnection patterns observed in the real atmosphere may be established through internal barotropic dynamical processes.

Key words: Preferred growing mode, Teleconnection pattern, Barotropic dynamical process

I. INTRODUCTION

Observational studies have shown that the variability of the anomaly relative to the climatological state in the atmosphere possesses multiple time scales, which is generally divided into three categories: high–frequency (period shorter than a week), low–frequency (period from about a week to a month or season) and ultra–low frequency (period longer than a month or season) variability. The atmospheric variability rises more from the low–frequency Cfromomponents than the high frequency components which are associated with the activities of fronts and cyclones (Blackmon, 1976). High frequency variability has been deeply understood that it mainly results from atmospheric internal baroclinic processes (Blackmon et al., 1979; Blackmon et al., 1984; Blackmon et al. 1984). However, we can be fair to say that the dynamical interpretation of low frequency variability has still been controversial. A fundamental problem, which is also the point at issue recent years, is if low–frequency variability may result as a consequence of external forcing or solely from internal dynamical processes. Observational studies and numerical experiments seem to have presented evidence that these two dynamical processes may both be important mechanisms to work (Horel and Wallace, 1981; Hoskins and Karoly, 1981; Hoskins and Ambrizzi, 1993; Lau, 1981; Simmons et al., 1983).

A substantial fraction of low–frequency variability consists several recurring, geographically fixed teleconnection patterns, which have equivalent barotropic structure and are intimately in relation to the Rossby wave energy dispersion (Wallace and Gutzler, 1981; Hsu and Lin, 1992). Generally, perturbations will interact with the basic flow. The Rossby wave energy dispersion and internal barotropic instability may thus jointly play an important role in the generation of teleconnection patterns. Such two mechanisms appear to have been separated in many dynamical studies. It is understandable that previous dynamical theories can only offer an explanation for some behavior of teleconnection patterns. In fact, for the real climatological flow with zonal and meridional variation, perturbations may extract kinetic energy from the background flow to grow, or be absorbed by the background flow (Lu and Zeng, 1981; Zeng, 1982). Therefore, only such perturbations which can efficiently extract kinetic energy from the basic flow during their propagation will develop significant

teleconnection patterns. In the present study, the concept of preferred growing perturbation is introduced into the dynamics of teleconnection pattern so as to understand the role of internal dynamical processes in the generation of teleconnection patterns.

II. PREFERRED GROWING PERTURBATION AND FORMULATION

Consider a real N-dimensional dynamical system with state vector x, whose evolution equation is

$$\frac{dx}{dt} = F(x) \ . \tag{1}$$

The evolution of a small perturbation x' is controlled by the linearized counterpart of (1), which can be written as

$$\frac{dx'}{dt} = Lx' \ . \tag{2}$$

where L is the Jacobian of F evaluated at a prescribed time t. Integrating over some portion of the trajectory from t_0 to t_1, we can write (2) in integral form

$$x'(t_1) = A(t_1,t_0)x'(t_0), \tag{3}$$

where $A(t_1,t_0)$ is a linear operator, which is called the resolvent of (2) and only depends on L.

Let $\langle \cdot , \cdot \rangle$ denote the inner product and $\| \cdot \|$ the associated norm. we can naturally define an amplification factor:

$$\sigma = \|x'(t_1)\| / \|x'(t_0))\|. \tag{4}$$

Obviously, the larger the σ, the more rapidly the perturbation grows in the energy sense. A perturbation may grow if $\sigma > 1$, which is called finite-time instability; A perturbation will decay if $\sigma < 1$, which is called finite-time stability; the energy of a perturbation will not be changed if $\sigma = 1$, which is called neutral instability (Molteni and Palmer, 1993).

From (3), the norm of x at time t_1 can be given

$$\|x'(t_1)\|^2 = (A(t_1,t_0)x'(t_0),\ A(t_1,t_0)x'(t_0)). \tag{5}$$

Thus, we have from (5)

$$\|x'(t_1)\|^2 = \Big(A^*(t_1,t_0)A(t_1,t_0)x(t_0),\ x(t_0)\Big), \tag{6}$$

where A^* is the adjoint of A.

Though A is an asymmetrical matrix, it can easily be shown that A^*A is a positive symmetrical matrix. We introduce a eigenvalue problem,

$$A^*Av = \lambda^2 v \ . \tag{7}$$

(7) is also called the singular value problem associated with A. Correspondingly, v is referred to as a singular vector, and λ^2 a singular value. It is a fundamental theorem of functional analysis that the eigenvectors of a symmetrical matrix such as A^*A can be chosen to form a complete orthonormal basis. Let $v_1, v_2, \cdots\cdots, v_N$ denote the eigenvectors and $\lambda_1^2, \lambda_2^2, \cdots\cdots, \lambda_N^2$ the associated eigenvalues, and suppose that the eigenvalues are arranged so that $\lambda_1^2 > \lambda_2^2 > \cdots\cdots > \lambda_N^2$.

A given initial perturbation $x(t_0)$ can be expanded in terms of v_j:

$$x'(t_0) = \sum_{j=1}^{N} a_j v_j \ , \tag{8}$$

$a_j = \langle x'(t_0),\ v_j \rangle$ is the projection of the perturbation $x'(t_0)$ onto v_j. Substituting (8) into (6) and utilizing the orthonormality between singular vectors, we get

$$\|x'(t_1)\|^2 = \sum_{j=1}^{N} a_j^2 \lambda_j^2 \ . \tag{9}$$

Thus,

$$\sigma^2 = \left(\sum_{j=1}^{N} a_j^2 \lambda_j^2 \ / \ \|x'(t_0)\|^2 \right) . \tag{10}$$

From (8), we obtain easily

$$\|x'(t_0)\|^2 = \sum_{j=1}^{N} a_j^2 \ . \tag{11}$$

It follows from (10) and (11) that the amplification factor to a given perturbation is determined by the magnitude of the singular values and the projections of the perturbation onto the singular vectors (the former is the reflection of the influences of the basic state, the later the reflection of the role of the structures of the perturbation itself). The larger the projections of a perturbation on singular vectors with large singular values, the larger amplification factor it has.

If an initial perturbation $x'(t_0)$ is parallel to a singular vector v_j, we can find from (10)

$$\sigma_j = \lambda_j \ . \tag{12}$$

(12) is of important interest. It indicates that if an initial perturbation $x'(t_0)$ is parallel to a singular vector associated with a large singular value, the amplification factor is large. Therefore, a singular vector associated with a large singular value is also referred to as a preferred growing mode.

From (7), we can also obtain

$$AA^*(Av) = \lambda^2 (Av) \ . \tag{13}$$

Since AA^* is a positive symmetrical matrix, so the time evolution of a singular vector Av is the eigenvector of AA^* and all the eigenvectors also form a complete orthogonal set. Thus, we can discuss the respective time evolution of different singular vectors.

In order to resolve the eigenvalue problem (13), we define the adjoint of (2),

$$-\frac{dx^*}{dt} = L^* x^* \ , \tag{14}$$

where L^* is the adjoint of L. Integrating (14) backward in time from t_1 to t_0, the solution can be written in integral form

$$x^*(t_0) = S(t_0, t_1) x^*(t_1) \ . \tag{15}$$

The subtraction of the inner product of (2) with respect to x^* from the inner product of (14) with respect to x' yields

$$\frac{d}{dt} \langle x'(t), x^*(t) \rangle = 0 \ . \tag{16}$$

So we have

$$< x'(t_1), x^*(t_1) > = < x'(t_0), x^*(t_0) > \quad . \tag{17}$$

Substituting (3) and (15) into (17), we obtain

$$< A(t_1, t_0) x'(t_0), x^*(t_1) > = < x'(t_0), S(t_0, t_1) x^*(t_1) > \quad . \tag{18}$$

Thus,

$$A^*(t_1, t_0) = S(t_0, t_1) \quad . \tag{19}$$

From (19), $A^* A x'(t_0)$ can be calculated as follows: first, we integrate (2) in time from t_0 to t_1 with initial value $x'(t_0)$, and have an integration value $x'(t_1)$; second, we integrate (13) backward in time from t_1 to t_0 with final condition $x'(t_1)$. The final integration value is just $A^* A x'(t_0)$. Therefore, using the power algorithm with orthogonalization (Feng, 1981), we can find the singular vectors and the singular values. The calculation processes can be outlined as follows:

Give an initial guess matrix $Y^0 = (x_{01}, x_{02}, \cdots, x_{0M})$, where Y^0 is a M × N matrix with perturbation vectors as columns. The orthogonality between all x_{0j} (j=1,2,$\cdots$,M) is required. M is the number of singular vectors which will be calculated, and $M \leqslant N$.

Compute

$$U^1 = A^* A Y^0 \quad .$$

Then, use Gramm–Shimidt algorithm to orthogonalize U^1. In fact, this orthogonalization corresponds to the linear transformation

$$Y^1 = U^1 R_1^{-1},$$

where R_1 is called an orthogonalizing matrix and is an upper triangular matrix.

Make iteration operations,

$$U^{n+1} = A^* A Y^n,$$

$$Y^{n+1} = U^{n+1} R_{n+1}^{-1},$$

where n is the iteration step. As iteration goes on, R_{n+1} will converge into a diagonal matrix. The diagonal elements are just the singular values which are arranged in descent order. The columns of Y^{n+1} are the corresponding singular vectors.

II. MODEL DESCRIPTION

The basic model used in this study is based on the damped barotropic vorticity equation

$$\frac{\partial \zeta}{\partial t} + J(\psi, \ \zeta + f) + \kappa \nabla^4 \ \zeta + \gamma \zeta = 0 \tag{20}$$

where $\zeta = \nabla^2 \psi$ is relative vorticity. $f = 2\Omega sin\varphi$, and ψ is streamifunction. φ is the latitude, and λ the longitude. J is the horizontal Jacobian operator. The variables are nondimensionalized as follows: time t by Ω^{-1}, length by a, ψ by $a^2\Omega$, where Ω and a are the angular velocity and the radius of the earth respectively

Linearizing about a zonally varying basic state, which is the climatological mean flow in this study, we can obtain the linearized equation

$$\frac{\partial \zeta'}{\partial t} + J(\bar{\psi},\ \zeta') + J(\psi',\bar{\zeta}+f) + \kappa\nabla^4\ \zeta' + \gamma\zeta' = 0, \tag{21}$$

where the climatological mean quantities are barred and the perturbation quantities are primed.

Introduce the kinetic energy inner product

$$\langle \zeta_a', \zeta_b' \rangle = \int_S \nabla\Delta^{-1}\zeta_a' \cdot \nabla\Delta^{-1}\zeta_b' dS. \tag{22}$$

where Δ^{-1} denotes the inverse operator of Laplacian operator ∇^2, and S is the entire atmosphere. We can obtain the adjoint of (21) with respect to this inner product

$$-\frac{\partial \zeta^*}{\partial t} = \nabla^2 J(\bar{\psi},\ \zeta^*) + J(\psi^*,\bar{\zeta}+f) - \kappa\nabla^4\ \zeta^* - \gamma\zeta^*\ . \tag{23}$$

Equation (21) and (23) are solved by representing all variables as series of spherical harmonics and triangular truncation is employed, so that

$$\zeta' = \sum_{m=0}^{J} \sum_{n=m}^{J} \left[\left(\zeta_n^m\right)^R cos(m\lambda) + \left(\zeta_n^m\right)^I sin(m\lambda)\right]\ P_n^m(\mu) \tag{24}$$

$$\zeta^* = \sum_{m=0}^{J} \sum_{n=m}^{J} \left[\left(\zeta_n^{*m}\right)^R cos(m\lambda) + \left(\zeta_n^{*m}\right)^I sin(m\lambda)\right]\ P_n^m(\mu) \tag{25}$$

Let $x = [\zeta_0^0,\ \zeta_1^0,\ \cdots, \left(\zeta_n^m\right)^R,\ \cdots, \left(\zeta_n^m\right)^I,\ \cdots]$, and correspondingly $x^* = [\zeta_0^{*0},\ \zeta_1^{*0},\ \cdots, \left(\zeta_n^{*m}\right)^R,\ \cdots, \left(\zeta_n^{*m}\right)^I,\ \cdots]$, where m = 1,2,···,21. In the following calculation processes, the fast Fourier transform and spectral–grid transform are applied. Considering the angular momentum conservation constraint, ζ_0^{*0}, ζ_1^{*0}, $\left(\zeta_1^1\right)^R$ and $\left(\zeta_1^1\right)^I$ should be taken as zero (Simmons et al. 1983). So x and x^* are the vectors of dimension N = (21+2)(21+1)−22−4 = 480. Then preferred growing modes can be found using the technique described in Section 2.

IV. ANALYSIS OF PREFERRED GROWING PERTURBATION

In the followings, we shall calculate and analyze the preferred growing modes and their time evolution. The basic state used in this study is the 300 hPa climatological mean flow in the northern winter, which comes from the 10 years of ECMWF analyses from 1980 to 1989. The dissipation coefficient is taken $\kappa = 4.772 \times 10^{16} m^4 s^{-1}$, so that the smallest wave in the model has damping time of 2 days. The Rayleigh friction coefficient is $\gamma = 8$ / day. For such parameters, normal analyses are performed, and the results are indicative of the stability of all the normal modes. In such a case, the development of normal modes is difficult to explain the generation of teleconnection patterns. Observational studies like Dole (1986) have shown that persistent anomalous patterns can be well established within a week. We thus take the evolution time of 4 days.

Table 1 presents the amplification factors of the first 12 preferred growing modes. It can be seen that the 12 modes all amplify. The amplitude of the first mode grows to 4.43 times as large as that of the initial perturbation during 4 days. The amplitude of the first three modes

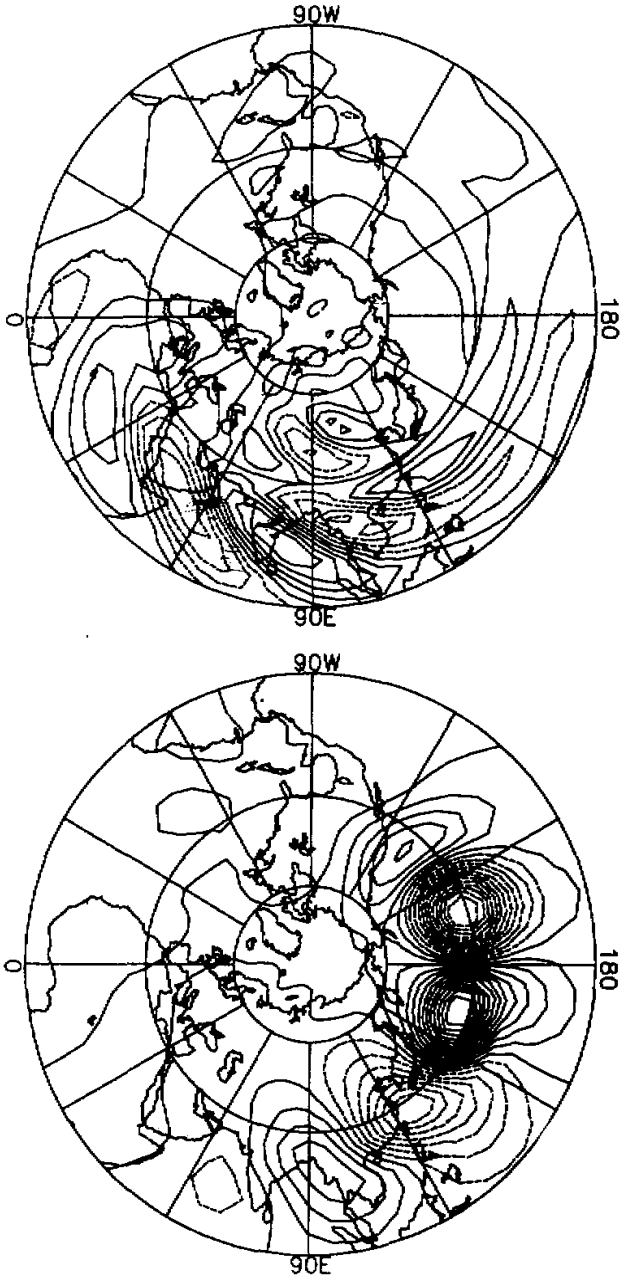

Fig. 1. (a) The streamfunction for the 1st preferred growing mode at initial time, and the contour interval is 0.1; (b) the structures of the teleconnection patterns at the evolution time of 4 days, and the contour interval is 0.4. The negative values are dashed, and nondimenesional unit is used.

increases by more than 3 times, whereas the 12th mode increases only by 1.85 times. Hence the growth rates are considerably different for different modes, which allows ones to distinguish preferred growing perturbations. In addition, the growth rates of the first several modes seem to be consistent with that of observed persistent anomalous patterns. It is noteworthy that a amplification factor is the growth rate averaged over the global domain. So the local growth rate can be expected to be much larger.

Table 1. The amplification factors of the first 12 preferred growing modes

Modes	1	2	3	4	5	6	7	8	9	10	11	12
Factors	4.43	3.99	3.03	2.88	2.74	2.65	2.38	2.32	2.08	2.07	1.93	1.85

In the following, we turn to the characteristics of the preferred growing perturbations.

Figure 1 shows the 1st preferred growing mode at the initial time and the time evolution at day 4. One can see that at the initial time the main perturbations are localized in the region from East Asia to the western Pacific. In fact, they are just localized to the region of the south of the Asian subtropical stream jet. These perturbations are characterized by so-called "leading wave" structure with the small spatial scale of about zonal wave number 7. Such characteristics seem to be consistent with those predicted by the wave packet theory (Lu and Zeng, 1981; Zeng, 1982). There is an indication from the wave packet theory that perturbations with such structures will efficiently extract kinetic energy from the stream jet. From the structure at day 4, it can be seen that the primary centers have propagated toward the northeast to the region from the western Pacific to the central Pacific. Day-by-day analyses indicate that such propagetion is realized through the establishment of new centers in succession downstream. Hence the propagation of the centers results from the Rossby wave energy dispersion. Compared with that at the initial time, the spatial scale of the centers at day 4 remarkably becomes larger. The main perturbation centers have the spatial scale of about zonal wave number 4. The analyses are indicative of a rapid strengthening of the strongest center. The strength of the strongest center increases by around 10 times. The structure at day 4 is similar to the teleconnection pattern called "East Asia / Pacific" (EAP) pattern. This is a teleconnection pattern of interest to Chinese meteorologists, and has been discussed in observational and theoretical studies (Hsu and Lin, 1992; Hoskins and Ambrizzi, 1993). The 2nd preferred growing mode has the structure resemblance to the 1st one except for $\pi / 4$ out of phase.

Figure 2 presents the 3rd preferred growing mode. It can be seen that the initial perturbations are mainly localized in the region from the western Pacific to the central Pacific and the North Africa region. It is of interest to note that the perturbations in the North Africa region is just localized to the region of the south of a relatively strong westerlies area. By day 4, two teleconnection patterns can be found. One is the typical southern Eurasian continent (SEA) pattern (Hsu and Lin, 1992). In a similar way to the East Asia / Pacific pattern, the main perturbations propagate eastward along the south of the Asian jet. The other has a resemblance to the Pacific / North America (PNA) pattern (Wallace and Gutzler, 1981; Blackmon et al., 1984). This pattern develops from the initial perturbations located in the region from the western Pacific to central Pacific, which propagate toward the northeast along

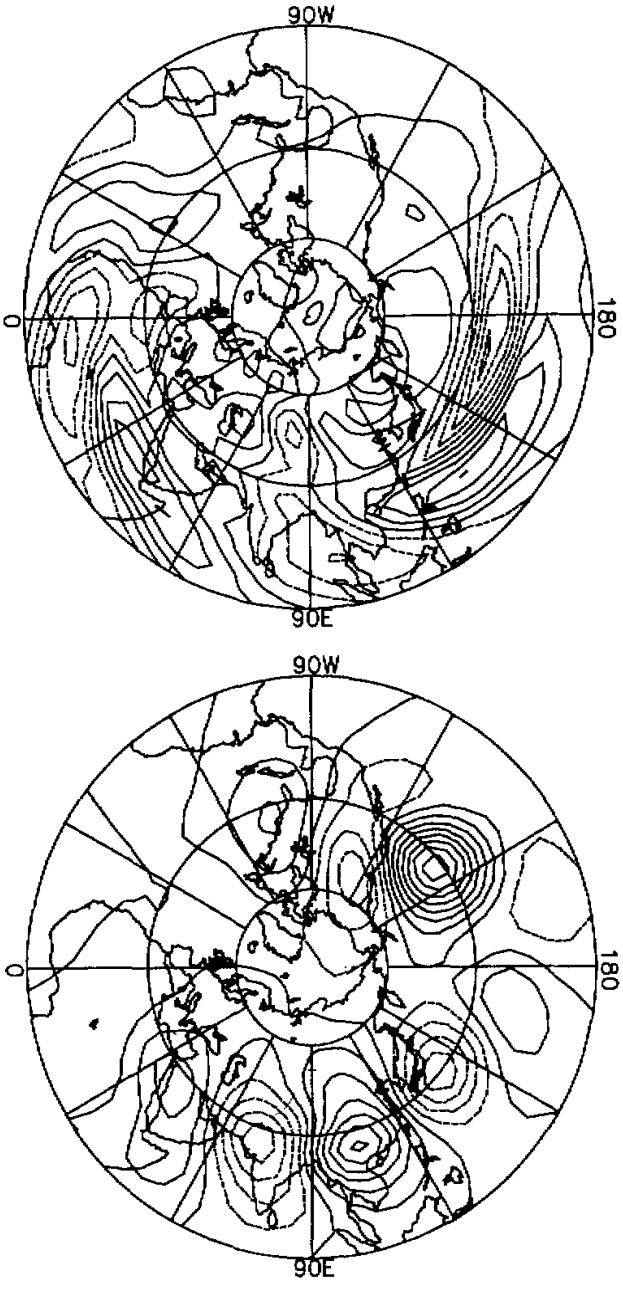

Fig. 2. Same as in Fig.1 but for the 3rd preferred growing mode.

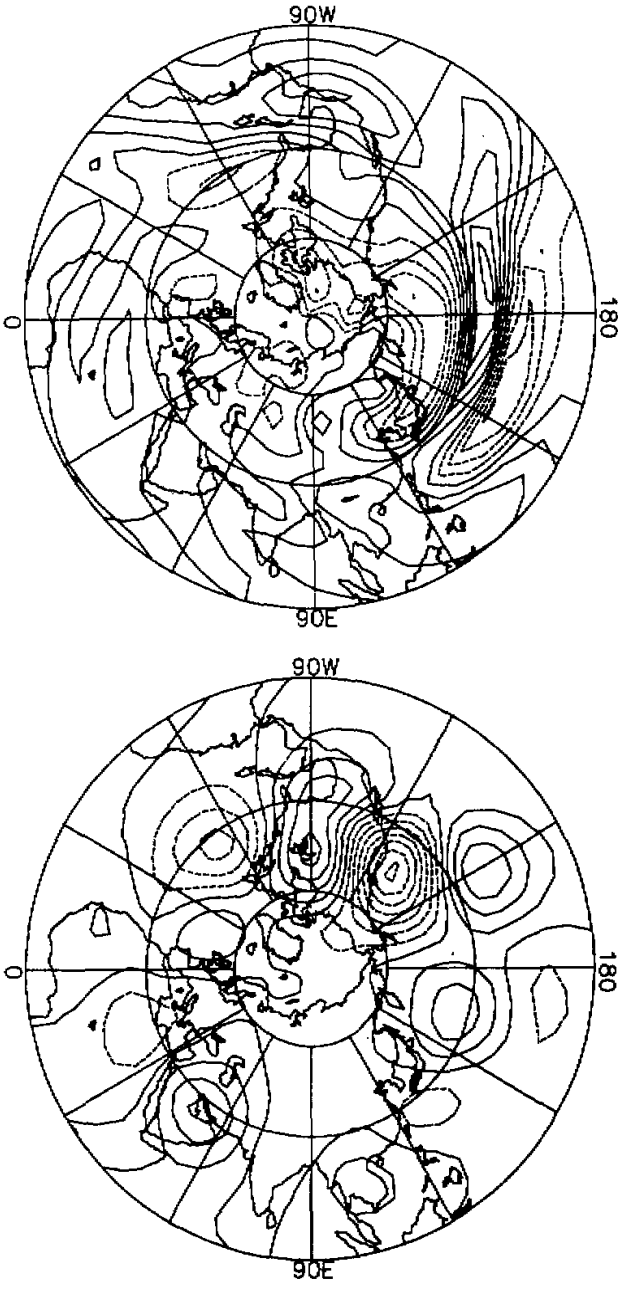

Fig. 3. Same as in Fig.1 but for the 5th preferred growing mode.

the exit area of the Asian jet with an increase in strength by about 5 times. It can be inferred that the exit area of the jet is a region in which perturbations may efficiently extract kinetic energy from the jet, which is the same as the finding by Simmons, et al. (1983). The 4th mode has similar structure to the 3rd mode but for $\pi / 4$ out of phase.

Figure 3 displays the 5th preferred growing mode and its time evolution. It can be seen that the initial perturbations are mainly localized in the regions from the western Atlantic to the central Atlantic and from South America to the western Atlantic. The structure at day 4 is characterized by the PNA pattern and the western Pacific (WP) pattern (Wallace and Gutzler, 1981). They develop from the perturbations over the western Pacific / the central Pacific. The perturbations from South America to the western Atlantic evolve into the western Atlantic (WA) pattern (Wallace and Gutzler, 1981; Blackmon et al., 1984).

The 6th preferred growing mode is presented in Fig. 4. It can be seen that the main initial perturbations are localized in three regions., i. e. North Africa, the central Pacific and South America / the western Atlantic. The perturbations localized in the former two regions develop the SEA pattern and PNA pattern respectively with the increase in the amplitude of the main centers by about 3 times. As is known, there is a stream jet from North America to the western Atlantic, called the Atlantic jet. The perturbations in the region from South America to the western Atlantic are just localized to the region of the south of the Atlantic jet. These perturbations develop the WA pattern through extraction of kinetic energy from the jet and propagation along the south of the jet.

Figure 5 shows the 7th preferred growing mode and its time evolution. One can see that the initial perturbations are mainly located over the western Pacific and in the region from South America to the western Atlantic, and relatively weak perturbations over North Africa. By day 4, a north–south oriented dipole teleconnection pattern is produced over the northeastern Pacific. This pattern bears a remblence to the PNA pattern for the time scale larger than a month (Blackmon et al., 1984). The SEA pattern is also noticed. In addition, the eastern Atlantic (EA) pattern has been established. In a similar way to the WA pattern, the EA pattern develops from the initial perturbation located in the region from South America to the western Atlantic which propagates along the region of the south of the Atlantic jet.

It is of interest to note that the initial preferred growing perturbations developing the PNA pattern have similar structures to the initial perturbations leading to the persistent anomalous pattern over the northern Pacific shown by Dole (1986). It should be pointed out that no European (EU) pattern (Wallace and Gutzler, 1981) is given in the preferred growing modes. However, if longer time evolution is considered, one can find that the EU pattern may develop from the EA pattern or the WA pattern through the Rossby wave energy dispersion downstream. In the analyses of the preferred growing modes for the northern summer (Li and Ji, 1995), it has been found that the initial perturbations located in the region from South America to the central Atlantic may develop the EU pattern by day 8.

VI. CONCLUSION AND DISCUSSION

From the analyses above, we have the following conclusions.

1) The growth rates of preferred growing modes may be close to those of the teleconnection patterns observed in the real atmosphere.

2) The most preferred growing modes all evolve into the teleconnection patterns consistent with the ones in the real atmosphere, and conversely all the main observed teleconnection patterns can develop from the preferred growing perturbations.

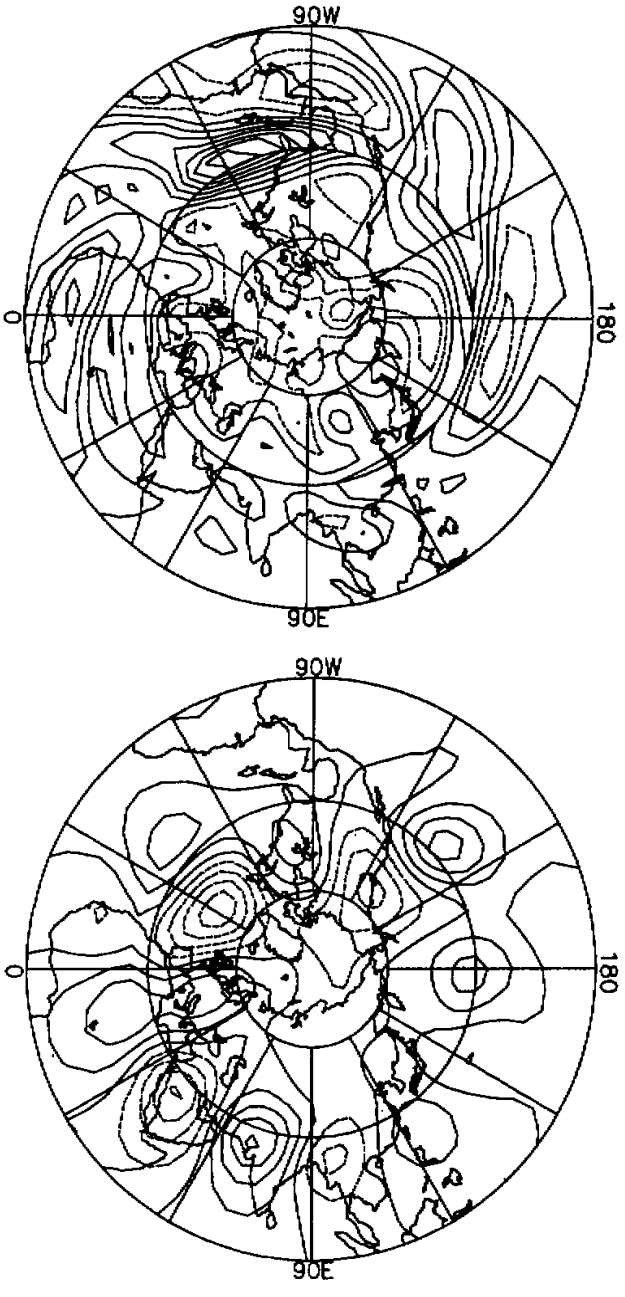

Fig. 4. Same as in Fig.1 but for the 6th preferred growing mode.

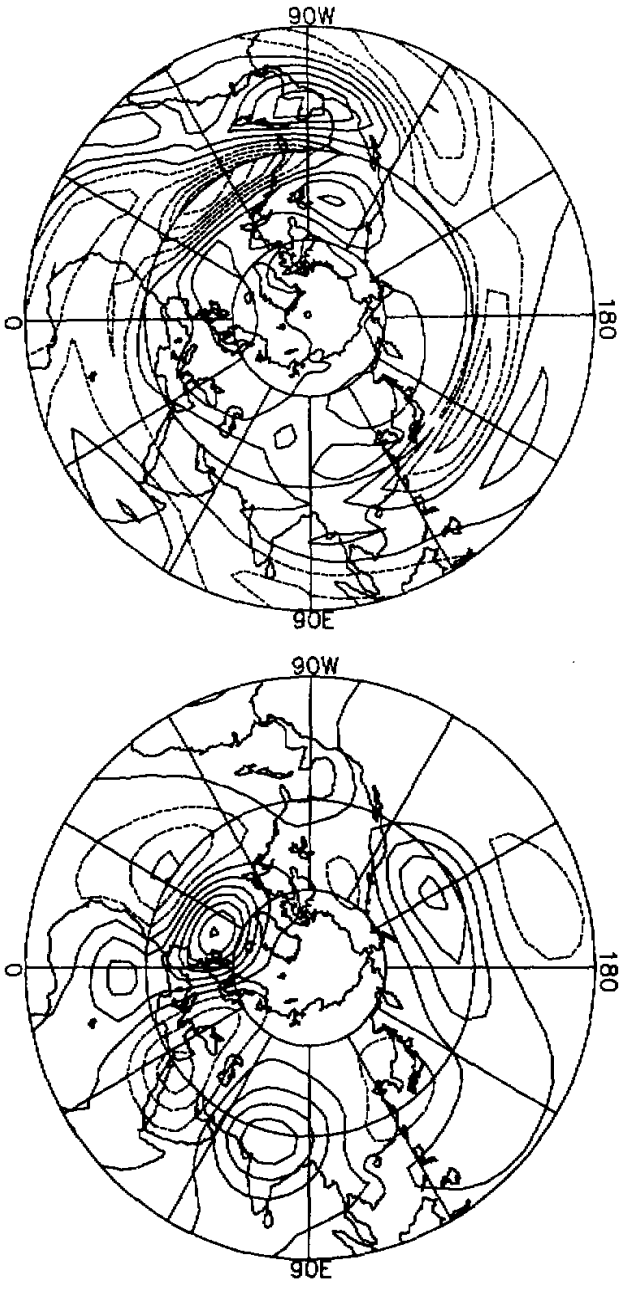

Fig.5 Same as in Fig.1 but for the 7th preferred growing mode.

3) The preferred growing perturbations located in the region from the western Pacific to the central Pacific at the initial time produce the PNA pattern or the WP pattern, which depends on the structures of the perturbations; The perturbations from South America to the western Atlantic develop the WA pattern, the EA pattern or the EU pattern, which also depends on the structures of the perturbations; the perturbations over North Africa produce the SEA pattern; the perturbations from East Asia to the western Pacific produce the teleconnection pattern associated with the EAP pattern.

4) The preferred growing perturbations are mainly localized to the region of the south of the strong flow with the "leading wave" structure at the initial time. They propagate along the south of the jets or the exit area of the jets and efficiently extract kinetic energy from the jets.

The conclusions above indicate that the development of main observed teleconnection patterns in the real atmosphere may only depend on the internal barotropic dynamics of the zonally-varying climatological flow, and they develop through the preferred growing perturbations which have much larger growth rates than normal modes. These perturbations choose such a path that they can most efficiently extract kinetic energy from the basic state during the propagation. Thus, the development of teleconnection patterns results from the coupled effect of the Rossby wave energy dispersion and the extraction of kinetic energy from the basic flow. This coupled effect favors most the rapid amplification of perturbations. As pointed out earlier, atmospheric low-frequency variability results primarily from the activities of teleconnection patterns. It can be inferred that internal barotropic dynamics plays a key role in low-frequency variability through developing persistent anomalous teleconnection patterns.

The authors are grateful for the helpful discussion with Profs. Chou Jifan, Li Chongyin and Wu Guoxiong. This research is supported by the National Natural Science Foundation for young scientists.

REFERENCES

Blackmon, M.L. (1976), A climatological spectral study of the 500 mb geopotential height of the Northern Hemisphere, *J. Atmos. Sci.*, **33**: 1607–1623.

Blackmon, M.L., R.A. Madden, J.M. Wallace and Gutzler, D.S. (1979), Geographical variations in the vertical structure of geopotential height fluctuations, *J. Atmos. Sci.*, **36**: 2450–2466.

Blackmon, M.L., Y.-H. Yee and J.M. Wallace (1984), Horizontal structure of 500 mb height fluctuations with long, intermediate and short time scales, *J. Atmos. Sci.*, **41**: 981–991.

Blackmon, M.L., Y.-H. Yee, J.M. Wallace and H.-H. Hsu (1984), Time variation of 500 mb height fluctuations with long, intermediate and short time scales as deduced from lag-correlation statistics, *J. Atmos. Sci.*, **41**: 961–979.

Dole, R.M. (1986), The life cycles of persistent anomalies and blocking over the northern Pacific, *Rev. Geophys.*, **29**: 31–69.

Feng, K. (1981), *Methods in Numerical Computation*, National Defense industrial Press, Beijing, P. 402–420 (in Chinese).

Horel, J. D. and J.M., Wallace (1981), Planetary scale atmospheric phenomena associated with the Southern Oscillation, *Mon. Wea. Rev.*, **109**: 2080–2092.

Hoskins, B.J. and D.J. Karoly (1981),The steady linear response of a spherical atmosphere to thermal and orographic forcing, *J. Atmos. Sci.*, **38**: 1179–1196.

Hoskins, B.J. and T. Ambrizzi (1993), Rossby wave propagation on a realistic longitudinally varying flow, *J. Atmos. Sci.*, **50**: 1661–1676.

Hsu, H. -H. S. -H. Lin (1992), Global teleconnections in the 250 mb streamfunction field during the Northern Hemispheric winter, *Mon. Wea. Rev.*, **120**: 1169–1190.

Lau, N. -C. (1981), A diagnostic study of recurrent meteorological anomalies appearing in a 15-year simulation with a GFDL general circulation model, *Mon. Wea. Rev.*, **109**: 2287–2311.

Li, Z., and L. Ji (1995), The preferred perturbations of growth in the brotropic atmosphere and development of teleconnections. Chinese *J. Atmos. Sci.* (to appear).

Lu, P. and Q.-C., Zeng (1981), Evolution of disturbances in the barotropic atmosphere, *Scientia Atmospheric Sinica.*, **5**: 1–8 (in Chinese).

Molteni, F. and T. N., Palmer (1993), Predictability and finite-time instability of the northern winter circulation, *Quater J. Roy. Meteor. Soc.*, **119**: 269–298.

Simmons, A. J., J. M. Wallace and G.W.Branstator (1983), Barotropic wave propagation, instability and atmospheric teleconnection patterns, *J. Atmos. Sci.*, **40**: 1263–1392.

Wallace, J. M., and D. S. Gutzler (1981), Teleconnections in the geopotential height field during the Northern Hemisphere winter, *Mon. Wea. Rev.*, **109**: 785–812.

Zeng, Q. -C. (1982), On the evolution and interaction of disturbances and zonal flow in rotation barotropic atmosphere, *J. Meteor. Soc. Japan*, **60**: 24–31.